JOURNAL OF SOLID STATE CHEMISTRY 61, 56–66 (1986)

Compound Formation, Crystal Chemistry, and Phase Equilibria in the System Li_3PO_4–$Zn_3(PO_4)_2$

G. TORRES-TREVIÑO AND A. R. WEST

University of Aberdeen, Department of Chemistry, Meston Walk, Old Aberdeen AB9 2UE, United Kingdom

Received March 26, 1985; in revised form June 12, 1985

The system Li_3PO_4–$Zn_3(PO_4)_2$ contains several new phases and solid solution series, some of which are interconvertible by high-temperature, composition-dependent, phase transitions. Crystal data are given for two of the new phases, α- and β-$Li_4Zn(PO_4)_2$. The β form appears to be structurally related to γ-Li_3PO_4, but with some cation disorder. The α form is ordered and appears to be structurally related to $Li_2Zn_3(SiO_4)_2$. The equilibrium phase diagram for this system has been determined.

Introduction

Solid solutions derived from γ-Li_3PO_4 and related materials such as γ-Li_3AsO_4, γ-Li_3VO_4, and Li_2ZnGeO_4 form the basis of a family of Li^+ ion conducting solid electrolytes (*1–6*). In these solid solutions, lower valent ions are substituted into the parent structure, together with extra Li^+ ions to preserve charge balance; it is the extra Li^+ ions that are responsible for dramatic increases in ionic conductivity. For instance, the conductivity of γ-Li_3PO_4 is $\ll 10^{-10}\ \Omega^{-1}\ cm^{-1}$ at room temperature but, on making the substitution $P^{5+} \rightleftarrows Si^{4+} + Li^+$, the conductivity rises by many orders of magnitude to reach a maximum of $\sim 1 \times 10^{-6}\ \Omega^{-1}\ cm^{-1}$ for compositions around $Li_{3.5}(Si_{0.5}P_{0.5})O_4$ (*1–3*). In all cases studied so far, the creation of extra, interstitial Li^+ ions led to increased conductivity. Only one brief study has been made on the effect of creating Li^+ vacancies in these structures and it did not lead to high conductivity (*7*). This involved making the substitution $2Li^+ \rightleftarrows Zn^{2+}$ in Li_2ZnGeO_4, to give $Li_{2-2x}Zn_{1+x}GeO_4$. On the other hand, in the related material Li_4SiO_4, creation of either interstitial Li^+ ions or Li^+ vacancies did give enhanced conductivity (*8*). The formulae of the two solid solutions involved were $Li_{4+x}(Al_xSi_{1-x})O_4$ [interstitial Li^+ ions] and $(Li_{4-3x}Al_x)SiO_4$ [Li^+ vacancies]; both involved the substitution of Al^{3+} into the structure but using two different mechanisms.

The present project began as an attempt to introduce Li^+ vacancies into Li_3PO_4 and to determine the effect, if any, on the conductivity. The system Li_3PO_4–$Zn_3(PO_4)_2$ was chosen for study and it turned out that a complex series of solid solutions and phases can be prepared. These results are reported here.

There appear to be no previous reports on the join Li_3PO_4–$Zn_3(PO_4)_2$ in the literature, although the end members are both

0021-4596/86 $3.00

well-known materials. Li_3PO_4 appears to exist in three polymorphic modifications, two of which can be retained to room temperature. The β polymorph appears to be the form that is thermodynamically stable at room temperature; it can be synthesized either by crystallization from aqueous solution (*9*) or by hydrothermal treatment of solid Li_3PO_4 at 250°C (*10*). It transforms to the γ polymorph on heating above ~420°C but the reverse transformation, $\gamma \rightarrow \beta$, is not observed on cooling (*11*). The transformation $\beta \rightarrow \gamma$ on heating is unusual since it takes place over a temperature range of ~40°C and shows evidence of martensitic character (*12*). The crystal structures of β- and γ-Li_3PO_4 are known (*9, 13*). Both are tetrahedral structures; the β structure is essentially an ordered Wurtzite (ZnS or ZnO) structure with Li and P atoms ordered over one set of tetrahedral sites within the essentially hexagonal close-packed (h.c.p.) array of oxide ions (*9*). In the γ structure, the oxide array is rather buckled (*13*) and may be described as either distorted h.c.p. or as a distorted form of the recently described tetragonal packing (t.p.) (*14, 15*). The Li and P atoms occupy tetrahedral sites but in a different manner to the β structure. Both sets of tetrahedral sites (within an ideally h.c.p. anion array) are used but overall these sites are only half full. A close relation between β and γ structures exists, therefore, and a topotactic mechanism for the transformation $\beta \rightarrow \gamma$ has been proposed which involves a simple, filled $\rightarrow$ empty tetrahedral site jump for half the cations in the structure (*16, 17*).

Between 1167°C and the melting point, 1205–1225°C (*18, 19*), a third polymorph of Li_3PO_4 has been reported to exist (*19*) from DTA results, although there appears to be no information on its structure. This polymorph has been labeled α (*19*). In Ref. (*19*), the polymorph that is stable below 1167°C has been labeled β and unfortunately, this is the polymorph labeled γ in the majority of the other publications including this one. Here we use the nomenclature:

$$\beta \xrightarrow{\sim 400^\circ C} \gamma \xrightarrow{1167^\circ C} \alpha$$

for the polymorphism of Li_3PO_4.

The naturally occurring form of Li_3PO_4, the mineral lithiophosphate (*20, 21*), is isostructural with the synthetic low temperature β polymorph (*9, 11*) although it was originally thought to be an olivine-like phase.

Zinc orthophosphate, $Zn_3(PO_4)_2$, appears to exist in two polymorphic modifications, α and β, stable below and above 942°C, respectively (*22*). The β polymorph is stable up to the melting point, 1060°C and, since the $\beta \rightarrow \alpha$ transition on cooling is sluggish, it can be retained readily to room temperature. The structures of both α and β polymorphs are known (*23, 24*); α is built of PO_4 and ZnO_4 tetrahedra that link up to form a 3D framework; β also contains PO_4 tetrahedra but the zinc coordination is rather more irregular and may be regarded as a mixture of 5- and 6-coordinated (*24, 25*).

A third, γ, polymorph of $Zn_3(PO_4)_2$ has been reported (*26*) but it requires the presence of a small concentration of other ions, e.g., Mg^{2+}, Mn^{2+}, and Cd^{2+} to stabilize it (*25, 26*). Its structure is known approximately (*27*) and also contains PO_4 tetrahedra with Zn^{2+} ions in 5- and 6-coordinate sites (*25*).

Experimental

Reagents used were Li_2CO_3, ZnO, and $(NH_4)_2HPO_4$; all were analar grade. The first two were dried at 300°C prior to weighing; $(NH_4)_2HPO_4$ was used directly from the bottle.

Initially, mixtures were prepared by weighing out the required amounts of starting material, giving a total of 5 to 10 g, which were then ground together in an agate mortar, using acetone or ethanol to

form a paste, dried, and fired. Firing was carried out in Pt crucibles or, for lithia-rich compositions, in a Au crucible, in air in electric muffle furnaces controlled and measured to ±25°C. A typical firing schedule was: 150 to 300°C, 12 hr and 600 to 800°C, 12 hr to expel gases followed by 1000 to 1100°C, 12 hr to complete the reaction. This procedure was found to be rather unsatisfactory, however, because free zinc oxide was often left after reaction.

The second preparative procedure that was tried, found to be suitable, and used for all subsequent work was to prepare initially quantities of Li_3PO_4 and $Zn_3(PO_4)_2$. These were then mixed in various ratios and reacted directly in Pt crucibles in the muffle furnaces at 900 to 1000°C for 1–2 days. The temperature used varied since it was found that compositions close to $Zn_3(PO_4)_2$ began to melt at a eutectic temperature of 900°C and it was necessary to avoid any melting during the preparation of bulk, stock samples. Weight loss checks were made on selected compositions and it was shown that lithia loss by volatilization was not a serious problem. For instance, Li_3PO_4-rich compositions, which melted at temperatures well above 1200°C, could be safely heated at 1100°C for 2–3 days.

These prereacted, stock samples were then used for phase diagram studies in order to observe the phase changes or reactions, if any, that occurred on changing temperature. For the phase diagram work, small samples, 50–100 mg, wrapped in Pt foil envelopes, were suspended in the hot zone of a vertical tube furnace whose temperature was controlled and measured to ±3°C by means of a Pt/Pt 13% Rh thermocouple placed in close proximity with the sample. At the end of each run, the samples could, if desired, be quenched to room temperature by dropping them into Hg.

In order to determine approximate melting temperatures, pelleted samples resting on Pt foil were placed in the muffle furnace at various temperatures in a stepwise heating cycle for 20 min each. The samples were removed while the furnace was heating up to the new temperature. With temperature increments of 25°C, melting temperatures could be determined reasonably accurately by noting the physical appearance of the pellets and, in particular, when slumping occurred. Knowledge of melting temperatures also helped in the assignment of DTA peaks.

Phase identification was carried out using X-ray powder diffraction with a Philips Hägg Guinier focusing camera, Cu$K\alpha_1$ radiation. For accurate d-spacing measurements, KCl (a = 6.2931 Å) was added as an internal standard and the films measured with a Cooksley microdensitometer. For DTA work, a Stanton Redcroft 675 Model was used with heating and cooling rates of 8°C min^{-1} and Al_2O_3 as inert reference material. Temperatures of heat effects were taken as the temperatures of peak maxima. Most transitions were rapidly reversible and the differences in peak temperatures between cooling and heating cycles were <20°C.

Results and Discussion

Compound and Solid Solution Formation; Phase Diagrams

In order to characterize the new phases and solid solutions that form on the orthophosphate join, Li_3PO_4–$Zn_3(PO_4)_2$, bulk samples of more than 50 different compositions were prepared. These were then subjected to a variety of furnace heat treatments, followed by rapid quenching or cooling at slower rates to room temperature. The products at room temperature were characterized by X-ray powder diffraction. A selection of the more important results is given in Table I.[1] Most composi-

[1] Tables I and II are part of a Ph.D. thesis (G. Torres-Treviño, University of Aberdeen) and may be obtained on request from the author.

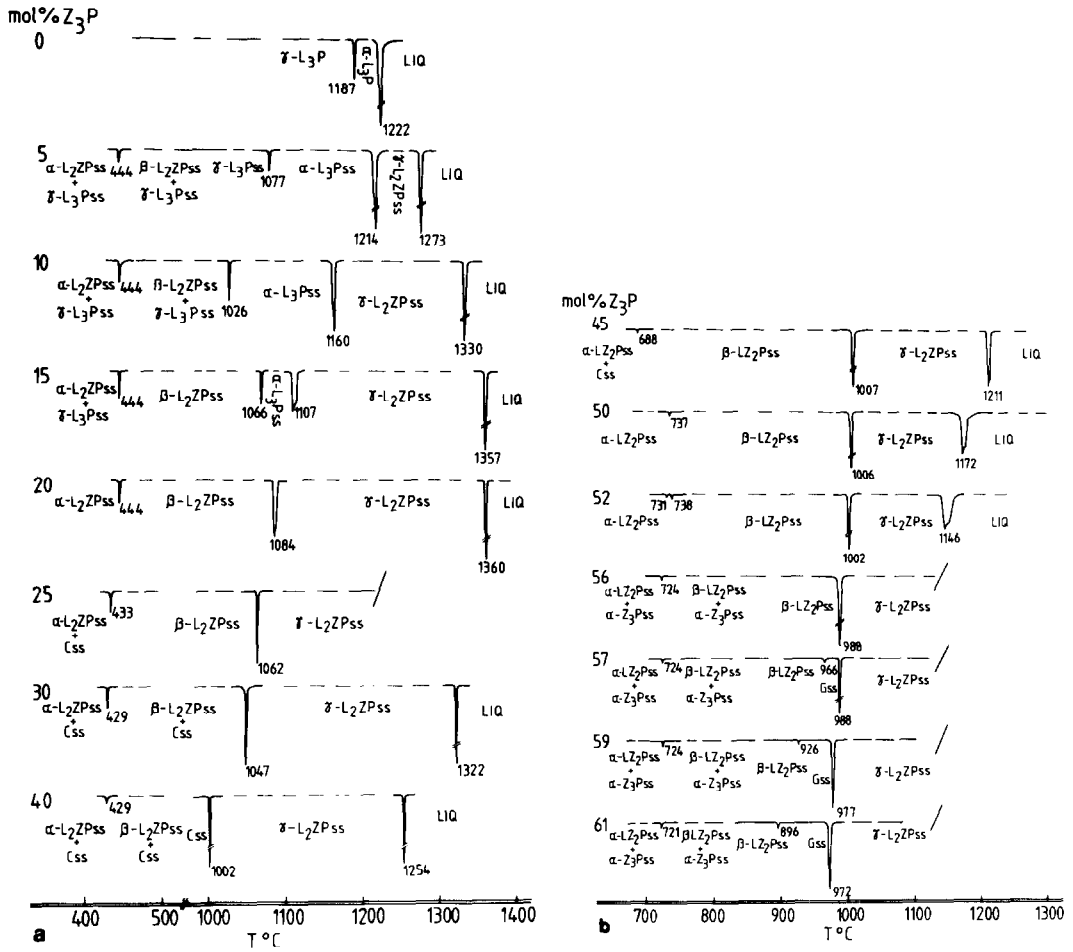

FIG. 1. Semischematic DTA traces obtained on heating Li, Zn orthophosphates. $L_3P = Li_3PO_4$, $L_2ZP = Li_4Zn(PO_4)_2$, $LZ_2P = LiZnPO_4$, $Z_3P = Zn_3(PO_4)_2$, ss = solid solution.

tions in the more complex region of the diagram, 0–60% $Zn_3(PO_4)_2$, were also studied by DTA. These results are given in Table II and a representative selection of DTA traces is shown in Fig. 1. These traces are semischematic in that although peak shapes and intensities are as indicated, variations in baseline with composition and/or temperature have been eliminated.

Using these X-ray and DTA results, the phase diagram shown in Fig. 2 was constructed. The phase diagram is complex and shows 11 solid solution series, many of which are interconvertible at a phase transition as a consequence of changing the temperature.

The principal factor which made determination of the phase diagram difficult was that most of the high-temperature phases and solid solutions could not be preserved, unchanged, to room temperature, even by rapid quenching into mercury; instead, they underwent transformation or decomposition reactions during cooling. Since we did not have high-temperature X-ray powder diffraction facilities available, the use of

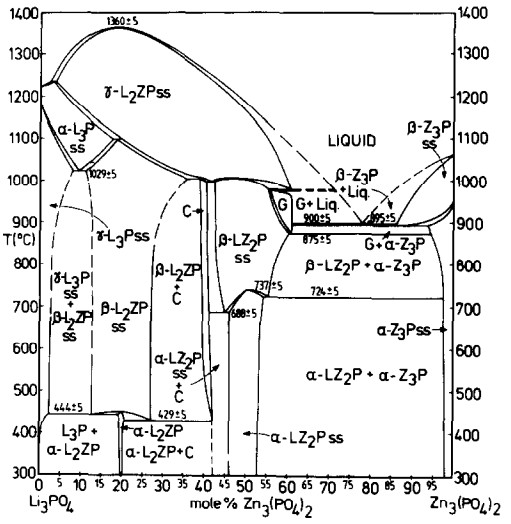

FIG. 2. Equilibrium phase diagram for the join, Li_3PO_4–$Zn_3(PO_4)_2$. Abbreviations as in Fig. 1.

DTA was critical to a successful determination of the phase diagram. For three of the solid solution phases, γ-$Li_4Zn(PO_4)_2$ ss, α-Li_3PO_4 ss, and β-$LiZnPO_4$ ss, we have no powder X-ray data since these phases cannot be quenched to ambient; their existence has been determined solely by DTA. For a fourth solid solution phase, β-$Li_4Zn(PO_4)_2$ ss, tentative X-ray data only are available since the $\beta \rightarrow \alpha$ transformation on cooling is only partially quenchable.

Solid lines on the phase diagram, Fig. 2, represent phase boundaries which were determined reasonably accurately either by quenching or DTA. Dashed lines represent phase boundaries which must exist but which have not been located accurately.

Starting from the Li_3PO_4 end of the diagram, only two polymorphs of Li_3PO_4 were encountered in this study, the α polymorph stable for a short range of temperatures below the melting point and the γ polymorph. Transformation of γ to β was not observed to occur, even on slow cooling, in accordance with previous observations (*9–12*). The γ polymorph is therefore kinetically stable to room temperature even though the thermodynamically stable polymorph below 350 to 400°C appears to be β. The transformation and melting temperatures of Li_3PO_4 were found, by DTA, to be

$$\gamma \underset{1162}{\overset{1187}{\rightleftharpoons}} \alpha \underset{1211}{\overset{1222}{\rightleftharpoons}} \text{liquid}$$

in reasonable agreement with the literature values (*18, 19*).

The γ and particularly the α polymorphs of Li_3PO_4 are able to dissolve appreciable amounts of $Zn_3(PO_4)_2$ in solid solution formation. The temperature stability field of α expands somewhat as the temperature of the $\gamma \rightleftarrows \alpha$ transition drops from ~1180°C in pure Li_3PO_4 to 1029°C with about 10% added $Zn_3(PO_4)_2$ and initially the melting point of α-Li_3PO_4 rises with added $Zn_3(PO_4)_2$.

At high temperatures, ≳1000°C, the phase diagram is dominated by an extensive range of solid solutions whose melting point passes through a maximum at a composition close or equal to 20% $Zn_3(PO_4)_2$ and 1360°C. The composition of maximum melting which corresponds to the formula, $Li_4Zn(PO_4)_2$, is presumed to be the ideal or stoichiometric formula on which this solid solution is based. In terms of oxide ratios, this formula is $2Li_2O \cdot ZnO \cdot P_2O_5$, abbreviated to L_2ZP, and the high-temperature polymorph has been labeled γ.

On cooling, γ-L_2ZP solid solutions undergo a variety of transformations, depending on composition. Over the range ~4 to 18% $Zn_3(PO_4)_2$, transformation to α-L_3P solid solution occurs initially with the transformation temperature decreasing gradually from 1234 to 1100°C over this range. Intermediate compositions, ~18 to ~34% $Zn_3(PO_4)_2$, transform to the solid solution phase labeled β-L_2ZP ss, which also supposedly has the ideal composition $Li_4Zn(PO_4)_2$. The α-L_3P solid solutions in the range ~12 to 18% $Zn_3(PO_4)_2$ also transform to β-L_2ZP solid solution on cooling.

The β-L_2ZP solid solutions are stable over a wide temperature range from 1000–1100°C down to 430–450°C. Below 430–450°C, further transformation occurs to give the phase α-L_2ZP. As far as could be determined, α-L_2ZP is essentially a line phase under conditions of thermodynamic equilibrium with a maximum extent of stable solid solutions in the range 19–21% $Zn_3(PO_4)_2$. Under nonequilibrium conditions, however, an extensive range of metastable α-L_2ZP solid solutions can be prepared, by transformation of the high temperature β solid solutions on cooling. Thus, the $\beta \rightarrow \alpha$ transformation cannot be prevented, even on quenching into Hg, but the associated exsolution of, e.g., Li_3PO_4 for compositions 11–19% $Zn_3(PO_4)_2$ takes place only slowly and is easily avoided by rapidly cooling the samples. In this way, metastable α-L_2ZP solid solutions may be prepared with compositions ranging from 11 to 27% $Zn_3(PO_4)_2$.

The existence of the thermodynamically stable line phase α-L_2ZP at composition 20% $Zn_3(PO_4)_2$ is an additional reason for treating this composition as a special composition and as the parent composition of the associated α, β, and γ solid solutions.

With increasing $Zn_3(PO_4)_2$ content, the next phase to appear at low temperatures is the phase labeled "C." It appears to exist over a narrow composition range, ~39–42% $Zn_3(PO_4)_2$, which is somewhat dependent on temperature. It also transforms above ~1000°C to γ-L_2ZP solid solutions.

At compositions centered around 50% $Zn_3(PO_4)_2$, a separate solid solution phase forms below ~1000°C which undergoes a polymorphic transformation below 688 to 737°C, depending on composition. Since the temperature of this transformation passes through a maximum at 50% $Zn_3(PO_4)_2$, there is some evidence for treating this as the ideal composition of the solid solution phase, with formula $LiZnPO_4$ abbreviated to LZ_2P. The low- and high-temperature polymorphs have been labeled α and β, respectively. The α phase forms over the composition range ~46–53% $Zn_3(PO_4)_2$, but depending on temperature, whereas the β phase is somewhat more extensive, ~43–60% $Zn_3(PO_4)_2$. At higher temperatures, $\gtrsim$1000°C, transformation to γ-L_2ZP solid solutions also occurs.

At compositions ~56–61% $Zn_3(PO_4)_2$ and temperatures of 875–975°C a solid solution phase labeled "G" forms. This phase can be quenched to room temperature, unlike most of the other high-temperature phases in this system.

At the $Zn_3(PO_4)_2$ end of the phase diagram, limited solid solutions form in the α and especially in the β polymorphs of $Zn_3(PO_4)_2$. The temperature of the $\alpha \rightleftarrows \beta$ transformation decreases somewhat with increasing Li_3PO_4 content.

The melting behavior of compositions on the join Li_3PO_4–$Zn_3(PO_4)_2$ has been studied only approximately using a combination of DTA and heat treatments on pressed pellets. The melting temperatures of the very extensive γ-L_2ZP solid solutions pass through a maximum at 20% $Zn_3(PO_4)_2$ and 1360°C. Melting temperatures pass through a minimum at a eutectic point, ~78% $Zn_3(PO_4)_2$, and 900°C. The join is a true binary join since at all temperatures and compositions the phase(s) that appear have a composition on the join Li_3PO_4–$Zn_3(PO_4)_2$.

In addition to the thermodynamically stable phases described above, which appear on the phase diagram, a metastable phase, labeled "D," forms on quenching liquids of composition ~70–80% $Zn_3(PO_4)_2$. There was no evidence of glass formation on quenching liquids in the present orthophosphate system and the formation of phase D probably represents an easier crystallization pathway than that of the eutectic crystallization reaction to give a mixture of phases, $Zn_3(PO_4)_2$ solid solution + phase G.

While Fig. 2 is an equilibrium phase dia-

gram and shows the phase(s) which exist as a function of composition at different temperatures, it is important to realize that many of the phase transitions that are shown take place rapidly. As a consequence the associated high-temperature phases undergo rapid transformation on cooling, even on quenching the samples into Hg. The following high-temperature phases could not be quenched to room temperature: γ-$Li_4Zn(PO_4)_2$ ss, α-Li_3PO_4 ss, β-$Li_4Zn(PO_4)_2$ ss, β-$LiZnPO_4$ ss. The only high-temperature phases which could, in fact, be quenched to room temperature were phase G and the high-temperature β polymorph of $Zn_3(PO_4)_2$ and its solid solutions.

Several of the solid solution series become markedly more extensive with increasing temperature and often, the high-temperature solid solutions could be quenched to room temperature in a supersaturated condition. The most clear example is the L_2ZP solid solutions mentioned earlier; although the $\beta \rightarrow \alpha$ transformation cannot be suppressed, the precipitation of either Li_3PO_4 (for compositions 11–18% $Zn_3(PO_4)_2$) or phase C (for compositions 22–27% $Zn_3(PO_4)_2$) is easily suppressed by rapid cooling. A similar but less dramatic effect was noticed in the LZ_2P solid solutions: the $\beta \rightarrow \alpha$ transition could not be avoided but precipitation of phase C and α-$Zn_3(PO_4)_2$ solid solutions on cooling Li_3PO_4-rich and $Zn_3(PO_4)_2$-rich compositions, respectively, could be suppressed. Similarly, the β- and α-$Zn_3(PO_4)_2$ solid solutions could be quenched intact, and, in this particular case, the $\beta \rightarrow \alpha$ transition did not occur on cooling either rapidly in Hg or more slowly in air. Finally, phase G could also be quenched intact.

In contrast to the above solid solutions, for which precipitation reactions on cooling took place only slowly, there was some evidence that both the γ-L_3P and β-L_2ZP solid solutions were considerably more extensive at high temperatures, ~1000°C, but that they underwent very rapid and unavoidable precipitation during cooling. Because of uncertainties over this and the precise extent of these solid solutions at ~800–1000°C, the solid solution limits in these regions of the phase diagram are shown dashed.

Crystal Chemistry of the Lithium Zinc Phosphates

Our information on the structures of the various new lithium zinc phosphate phases is limited, partly due to the lack of high-temperature X-ray data with which to characterize the high-temperature phases. At present we have partial structural data only for the phases α-$LiZnPO_4$, α-$Li_4Zn(PO_4)_2$, and β-$Li_4Zn(PO_4)_2$.

α-$LiZnPO_4$ has a large monoclinic unit cell (*28*) as determined by selected area electron diffraction, with parameters, a = 17.35, b = 9.79, c = 17.10 Å, β = 111.1°. The unit cell contains 32 formula units. From these data and the complex nature of the powder pattern of α-$LiZnPO_4$, it was concluded that it does not belong to one of the simple structure types shown by, e.g., $LiMgPO_4$ (olivine-like), $LiNiVO_4$ (spinel-like) or $LiZnAsO_4$ (phenacite-like). Attempts to grow crystals of size suitable for X-ray crystallographic studies were unsuccessful.

Single crystals of α-$Li_4Zn(PO_4)_2$ large enough for rotation and Weissenberg photographs were obtained from a sample of the same composition. The sample had been melted briefly by holding at 1380°C for 10 min and then slowly cooled to 1300°C over a period of 6 hr. Although the crystal chosen was, in fact, an aggregate of several crystals, it was possible to identify a side-centered orthorhombic cell from the X-ray photographs. The cell axes were chosen so that the conditions for reflection became hkl: $h + k = 2n$ together with $00l$: $l = 2n$, corresponding to space group, $C222_1$, No. 20. Using this information, the X-ray pow-

TABLE III

X-RAY POWDER DIFFRACTION DATA

d_{obs} (Å)	d_{calc} (Å)	*hkl*	*I*
	α-$Li_4ZnP_2O_8$		
Orthorhombic, space group $C222_1$ unit cell dimensions: $a = 12.885 \pm 0.008$ Å, $b = 9.901 \pm 0.005$ Å, $c = 10.286 \pm 0.006$ Å			
7.924	7.855	110	48
6.275	6.243	111	70
5.479	5.460	201	44
4.313	4.303	112	46
4.025	4.020	202	84
3.932	3.941	310	100
	3.928	220	
3.677	3.680	311	71
	3.669	221	
3.147	3.142	113	30
3.128	3.128	312	30
3.055	3.055	131	28
3.027	3.027	203	36
2.820	2.820	023	8
2.733	2.730	402	80
2.719	2.717	132	44
2.610	2.612	421	42
2.588	2.587	313	44
	2.583	223	
2.574	2.572	004	84
2.539	2.538	331	12
2.497	2.494	510	12
2.475	2.477	040	66
2.443	2.444	114	4
2.425	2.424	511	4
2.411	2.409	041	4
2.388	2.391	422	14
	2.388	204	
2.329	2.333	332	17
2.256	2.256	241	6
2.245	2.244	512	6
2.147	2.148	600	6
2.117	2.122	423	28
2.107	2.109	242	28
	2.102	601	
2.013	2.017	513	10
	2.010	404	
2.002	2.008	043	10
	2.004	134	
1.987	1.990	115	14
1.960	1.960	205	4
1.928	1.929	441	16
1.914	1.917	243	8
1.896	1.900	025	7
	1.890	532	

d_{obs} (Å)	d_{calc} (Å)	*hkl*	*I*
	β-$Li_4Zn(PO_4)_2$[a]		
Orthorhombic: $a = 6.441 \pm 0.004$ Å, $b = 4.960 \pm 0.004$ Å, $c = 10.252 \pm 0.006$ Å			
4.019	4.011	102	100
3.937	3.930	110	96
3.677	3.670	111	23
3.120	3.119	112	23
2.820	2.814	013	10
2.727	2.727	202	85
2.611	2.612	211	42
2.584	2.579	113	40
2.569	2.563	004	83
2.480	2.480	020	77
2.414	2.410	021	3
2.389	2.390	212	15
	2.382	104	
2.149	2.147	300	4
	2.147	114	
2.117	2.119	213	25
2.110	2.109	122	5
2.007	2.007	023	4
	2.005	204	
1.931	1.935	311	6
	1.930	221	
1.896	1.895	015	5
1.858	1.859	214	1
1.833	1.840	312	31
	1.835	222	
1.782	1.782	024	14

d_{obs} (Å)	*I*	d_{obs} (Å)	*I*
	Phase C $Li_9Zn_6(PO_4)_7$		
5.057	2	2.415[b]	22
4.037	100	2.350	7
3.973	100	2.264	7
3.704	25	2.126	30
3.541	10	2.108	25
3.348	1	2.027[b]	12
3.317	1	2.002	7
3.122	25	1.987	7
2.770[b]	37	1.947	5
2.663	20	1.908	10
2.654	20	1.884	5
2.565	17	1.866	7
2.517[b]	37	1.846	12
2.481	62	1.764	7

TABLE III—*Continued*

d_{obs} (Å)	I	d_{obs} (Å)	I
	Phase G, $LiZn_9(PO_4)_7$		
5.022	3	2.401	12
4.301[b]	25	2.383	8
4.058	100	2.348	20
3.994	53	2.337	8
3.555	23	2.319	8
3.405	4	2.153	15
3.213	78	2.136	15
3.197	23	2.081	9
3.135	8	2.026	3
3.071	8	1.989	15
2.942	3	1.975	15
2.822	27	1.956	3
2.732	4	1.924	3
2.642	4	1.897	19
2.529	53	1.869	5
2.496	1	1.850	7
2.471	7	1.832	3
2.436	22		
	Phase D, $LiZn_4(PO_4)_3$		
7.631	6	2.263	3
5.001	48	2.236	23
4.411	29	2.201	39
4.253	14	2.148	17
4.061	80	2.120	4
4.009	80	2.083	17
3.918	36	2.015	9
3.799	4	1.997	13
3.628	39	1.956[b]	17
3.542	4	1.934	14
3.452	4	1.900	9
3.243	91	1.882	17
3.191	4	1.856	1
3.134	4	1.818	7
3.052	100	1.718	12
2.940	44	1.661	9
2.831	3	1.616[b]	16
2.799	23	1.595	10
2.713	10	1.583	11
2.633[b]	45	1.574	15
2.584	7	1.537[b]	20
2.527	29	1.518	5
2.483[b]	30	1.492	15
2.444	13	1.479	9
2.419	9	1.455	12
2.377	20	1.441	15
2.338	1	1.430	15
2.311	7		

der pattern was indexed and refined cell dimensions obtained (Table III).

The detailed structure of α-$Li_4Zn(PO_4)_2$ is not known but it is related to that of the higher-temperature β polymorph by means of an order–disorder phase transition. Further, β-$Li_4Zn(PO_4)_2$ appears to be closely related structurally to γ-Li_3PO_4 and hence the α structure is an ordered form of a γ-Li_3PO_4 derivative structure. Evidence for these assertions is as follows.

The powder pattern of α-$Li_4Zn(PO_4)_2$ shows considerable similarities to that of phase C′, $Li_2Zn_3(SiO_4)_2$, an ordered orthosilicate solid solution phase that occurs in the system Li_4SiO_4–Zn_2SiO_4 (*29, 30*). Phase C′ undergoes a disordering transition at ~450°C and the high-temperature γ_{II} structure is one member of a solid solution series with Li_2ZnSiO_4 as the parent composition. γ_{II}–Li_2ZnSiO_4 is isostructural with γ-Li_3PO_4 (*29, 30*). Hence phase C′, $Li_2Zn_3(SiO_4)_2$, and the present new phase, $Li_4Zn(PO_4)_2$, have the same overall cation : anion ratio of 7 : 8 and appear to be derivative, γ-Li_3PO_4 structures.

It is not known if α-$Li_4Zn(PO_4)_2$ and $Li_2Zn_3(SiO_4)_2$ are, in fact, isostructural. Their powder patterns show considerable similarities but an indexing scheme for the $Li_2Zn_3(SiO_4)_2$, phase C′, pattern (*30*) used a halved *c* axis by comparison with the *b* axis of α-$Li_4Zn(PO_4)_2$ (Table III). [NB *a b c* for α-$Li_4Zn(PO_4)_2$ has the same setting as *a c b* for $Li_2Zn_3(SiO_4)_2$ (*30*)]. However, the powder data used in (*30*) were of poorer quality than those reported here, without an internal standard and without using least-squares refinement to aid in indexing. Further work is needed to determine/confirm the unit cell

[a] β-$Li_4ZnP_2O_8$ is stable above ~425°C and cannot normally be quenched to room temperature. This pattern was obtained on material that was stabilized to room temperature by partial substitution of (P + Li) for (Si + Zn) with an overall composition, $Li_{3.8}Zn_{1.2}P_{1.8}Si_{0.2}O_8$.

[b] Broad line.

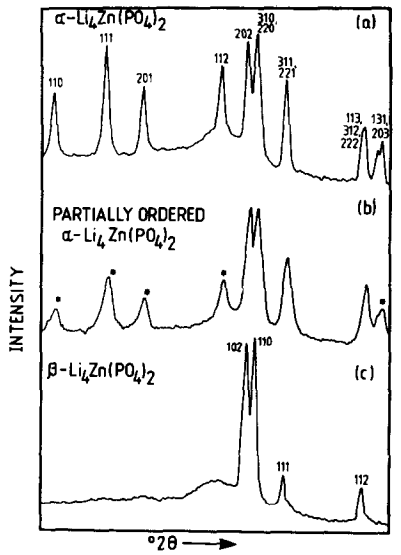

FIG. 3. X-Ray microdensitometer traces for two polymorphs of $Li_4Zn(PO_4)_2$. Asterisked lines exhibit broadening.

of phase C′, $Li_2Zn_3(SiO_4)_2$, therefore, and to show whether or not it is isostructural with α-$Li_4Zn(PO_4)_2$.

The phase β-$Li_4Zn(PO_4)_2$ cannot be quenched to room temperature but its powder pattern has been inferred by two methods and is given in Table III. First, preliminary studies of solid solution formation on the join $Li_4Zn(PO_4)_2$–$Li_2Zn_3(SiO_4)_2$ have been carried out. These showed that, for compositions close to $Li_4Zn(PO_4)_2$, e.g., with a mole ratio of 9:1 of the two end members, the powder pattern of the quenched product was very similar to that of α-$Li_4Zn(PO_4)_2$ (Fig. 3a), but with one set of lines absent (Fig. 3c). Second, on quenching samples of $Li_4Zn(PO_4)_2$ itself from temperatures $\gtrsim$425°C, one set of lines in the resulting powder pattern was seen to be markedly broadened (Fig. 3b). These lines, asterisked, correspond to those lines that were absent from the phosphate–silicate solid solution pattern (Fig. 3c). It was concluded, therefore, that the effect of adding $Li_2Zn_3(SiO_4)_2$ to $Li_4Zn(PO_4)_2$ was to at least partially stabilize the β phase, so that it could be quenched intact to room temperature. The powder pattern of β-$Li_4Zn(PO_4)_2$ given in Table III is that of the silicate-stabilized phase.

It seems likely that β-$Li_4Zn(PO_4)_2$ is structurally similar to, if not isostructural with, γ-Li_3PO_4. The a dimensions are rather different in the two phases which may account for the fact that the phase diagram, Fig. 2, does not show complete solid solution between them (i.e., covering the composition range 0–20% $Zn_3(PO_4)_2$ at ~450–1050°C). β-$Li_4Zn(PO_4)_2$ is cation-deficient by comparison with γ-Li_3PO_4. Also if β-$Li_4Zn(PO_4)_2$ is isostructural with γ-Li_3PO_4, the structure must possess considerable disorder since there are no twofold positions in space group *Pmnb* to accommodate the two Zn^{2+} ions. One possibility is that Zn^{2+} ions and vacancies are disordered over the fourfold Li(2) sites of the γ-Li_3PO_4 structure (*13*). In this case, the $\beta \rightarrow \alpha$ transition at ~425°C could well be associated with the ordering of the Zn^{2+} ions. A similar effect may occur in the $\gamma_{II} \rightarrow C'$ transition in $Li_2Zn_3(SiO_4)_2$ at ~450°C.

No structural information is available for the phases labeled C, G, and D; unindexed powder X-ray data are given for them in Table III.

Acknowledgment

G.T.T. thanks CONACYT, Mexico, for a studentship.

References

1. Y.-W. HU, I. D. RAISTRICK, AND R. A. HUGGINS, *J. Electrochem. Soc.* **124**, 1240 (1977).
2. R. D. SHANNON, B. E. TAYLOR, A. D. ENGLISH, AND T. BERZINS, *Electrochim. Acta* **22**, 783 (1977).
3. R. A. HUGGINS, *Electrochim. Acta* **22**, 773 (1977).
4. A. KHORASSANI AND A. R. WEST, *Solid State Ionics* **7**, 1 (1982).
5. A. KHORASSANI AND A. R. WEST, *J. Solid State Chem.* **53**, 369 (1984).

6. H. Y.-P. Hong, *Mater. Res. Bull.* **13,** 117 (1978).
7. P. G. Bruce and A. R. West, *J. Solid State Chem.* **44,** 354 (1982).
8. K. Jackowska and A. R. West, *J. Mater. Sci.* **18,** 2380 (1983).
9. C. Keffer, A. Mighell, F. Mauer, H. Swanson, and S. Block, *Inorg. Chem.* **6,** 119 (1969).
10. P. Tarte, *J. Inorg. Nucl. Chem.* **29,** 915 (1967).
11. A. R. West and F. P. Glasser, NBS Spec. Publ. 364, "Solid State Chemistry," p. 457 (1972).
12. C. Ibarra-Ramirez, M. Villafuerte, and A. R. West, *J. Mater. Sci. Lett.* **20,** 812 (1985).
13. J. Zemann, *Acta Crystallogr.* **13,** 863 (1960).
14. A. R. West and P. G. Bruce, *Acta Crystallogr. B* **38,** 1891 (1982).
15. W. H. Baur, *Mater. Res. Bull.* **16,** 339 (1981).
16. A. R. West, *Nature (London)* **249,** 245 (1974).
17. A. R. West, *Z. Krist.* **141,** 422 (1975).
18. T. Y. Tien and F. A. Hummel, *J. Am. Ceram. Soc.* **44,** 206 (1961).
19. R. K. Osterheld, *J. Inorg. Nucl. Chem.* **30,** 3173 (1968).
20. W. S. Matias and A. Bondareva, *Dokl. Akad. Nauk, S.S.S.R.* **112,** 124 (1957).
21. D. J. Fischer, *Amer. Mineral.* **43,** 761 (1958).
22. F. L. Katnack and F. A. Hummel, *J. Electrochem. Soc.* **105,** 125 (1958).
23. C. Calvo, *Canad. J. Chem.* **43,** 436 (1965).
24. J. S. Stephens and C. Calvo, *Canad. J. Chem.* **45,** 2303 (1967).
25. A. G. Nord and P. Kierkegaard, *Chem. Scripta* **15,** 27 (1980).
26. A. L. Smith, *J. Electrochem. Soc.* **98,** 363 (1951).
27. C. Calvo, *J. Phys. Chem. Solids* **24,** 141 (1963).
28. J. A. Gard, G. Torres-Treviño, and A. R. West, *J. Mater. Sci. Lett.* **4,** 1138 (1985).
29. A. R. West and F. P. Glasser, *J. Mater. Sci.* **5,** 557 (1970).
30. A. R. West and F. P. Glasser, *J. Mater. Sci.* **5,** 676 (1970).